An electrochemical comparison of thiolated selfassembled monolayer (SAM) formation and stability in solution on macro and nanoelectrodes

RESEARCH ARTICLE
doi.org/10.1002/elsa.202100077

Chemistry Europe
European Chemical Societies Publishing

Received: 30 April 2021
Revised: 21 July 2021
Accepted: 22 July 2021

An electrochemical comparison of thiolated self-assembled monolayer (SAM) formation and stability in solution on macro- and nanoelectrodes

Andrew Piper[1] | **Damion K. Corrigan**[2] | **Andrew R. Mount**[1]

[1] EaStCHEM, School of Chemistry, The University of Edinburgh, Edinburgh, UK
[2] Department of Biomedical Engineering, University of Strathclyde, Glasgow, UK

Correspondence
Andrew Piper, EaStCHEM, School of Chemistry, The University of Edinburgh, Joseph Black Building, The King's Buildings, West Mains Road, Edinburgh, EH9 3JJ, Scotland, UK.
Email: andrewpiper89@gmail.com

Funding information
University Of Edinburgh

Abstract

Thiolated self-assembled monolayers (SAMs) formed on metal electrodes have been a topic of interest for many decades. One of the most common applications is in the field of biosensors, where this is a growing need for functionalizing nanoelectrodes to realize more sensitive and implantable sensors. For all these applications, the SAM-functionalized nanoelectrodes will need to make reliable and interpretable electrochemical measurements. In this work, electrochemical impedance spectroscopy (EIS) is used to monitor both the formation and subsequent stability of 6-mercaptohexan-1-ol SAMs on macro and nanoelectrodes and compares the two. To develop effective devices, it is crucial to understand both SAM formation and the resulting signal stability on nanoscale surfaces and this is done by comparing to behaviors observed at the well-understood macroscale. We report an initial stochastic binding event and subsequent re-arrangement of the SAMs for both electrode types. However, this re-arrangement takes hours on the macroscale electrodes but only seconds on the nanoelectrodes. This is proposed to be due to the different structures of the SAMs on the electrodes predominantly driven by their bulk-to-edge ratios. After formation, the SAMs formed on both macro- and nanoelectrodes exhibit significant instability over time. The reported results have practical implications for the construction of SAM-based biosensors on macro- and nanoscale electrodes.

1 | INTRODUCTION

Nanoscale electrodes are a topic of growing interest in the field of biosensors where there is a drive to miniaturize electrodes to realize implantable sensors and enhanced sensor performance.[1] To achieve these applications, it is important to add functionality to nanoscale electrodes. The current *modus operandi* for functionalizing electrodes is to spontaneously form self-assembled monolayers (SAMs) with alkanethiols.[2] Normally, the electrode is immersed in an organic solvent containing μM to mM concentrations of the desired thiol. This is then usually left for several hours[3] or overnight.[1e] The processes taking place during this time have been the subject of investigation for several decades. Notably works by Poirier[4] and Brett[3] have looked into the structures of SAMs as their concentrations on an electrode increase and at methods of accelerating the SAM formation process respectively. As well as this, the stability of the electrode material (commonly Au) has been studied in depth for the hours and days

RESEARCH ARTICLE
doi.org/10.1002/elsa.202100077
Chemistry Europe
European Chemical Societies Publishing

after SAM formation.[4–5] Most of these studies make use of STEM,[4] He diffraction,[6] STM[7], AFM,[8] or XPS[7c] with little characterization by electrochemical methods being reported.[5]

The current state of the art theory is that the thiols (RSH) thioesters (RSR) and disulfides (RSSR), deposited from the solution undergo a two-step binding process to the electrode surface.[7c,9] There is an initial physisorption step followed by chemisorption in which covalent Au-S bonds are formed.[8b] During this second step, there is a rearrangement of the surface as pits form in the electrode and the SAMs aggregate to form islands.[4,8b,10] AFM studies by Xu et al[8b] show that the phase of the SAM formed from solution changes as a function of coverage, there is an initial formation of a lying down phase that over time aggregates to form SAM islands in the standing up phase with a 30° offset from the normal.[8b]

This rearrangement is dependent on the deposition conditions and the underlying substrate and can be accelerated by applying a voltage (or series of voltage pulses) to the electrode.[3] The end result of this rearrangement is a SAM monolayer in what Poirier defined as the "Φ-phase" or a standing up phase,[4] in which a one-third surface coverage by a monolayer in a $(\sqrt{3} \times \sqrt{3}R30°)$ geometry is obtained. The electrode itself is electrochemically active through pinholes or defects in this surface monolayer.[2a] It has been reported that thiols bound to the electrode surface are aggregate into islands on the surface and create pits within the electrodes, both of which evolve over time and are dependent on the crystal structure of the electrode,[7a,7c,10b,11] time,[7a,10b,12] temperature,[10b] solvent,[10a] and SAM chemistry.[10a] To date the majority of the research done in the field is on Au-S systems, however in this project Pt-S systems are investigated. This is not without precedent,[13] the two systems have previously been shown to be comparable by Whitesides et al.[14]

To date, the main analysis of SAM formation on the nanoscale has been performed in the study of "nanografting."[15] A process by which nanoscale pinholes are created in SAM films and then backfilled with a different SAM (typically a biomolecular probe) in order to try and control the placement of probes on an electrode surface.[15] It has been observed that this backfilling has enhanced kinetics over the initial SAM formation due to spatial-confinement effects, where the surrounding SAM being in the upright as opposed to lying down configuration increases the rate of binding.[8c,16] Or, to put it another way, when a single thiol is removed from a film at equilibrium; any thiol added to replace it will bind at an accelerated rate as it will bind into the most thermodynamically stable conformation as it does not need to undergo any rearrangement.

Once formed the stability of the SAM is important. For decades now it has been observed that over the course of days a metal/thiolate interface will rearrange and restructure to create holes in the metal.[4,10b] This is achieved because the thiol-metal bond is so strong that it creates adatoms on the metal surface, these S-metal adatom complexes are themselves mobile at the surface-SAM interface and aggregate over time causing the formation of SAM islands and pits in the metal structure.[17] Given that functionalized electrodes are often used for electroanalysis, it is important to understand how the electrochemical signal changes as SAM layers are formed as well as their stability over time. It is the purpose of this paper to further understand and report the electrochemical properties of metal-thiolate self-assembled monolayers on macro- and nanoelectrodes and explain the differences between them during both SAM formation and subsequent SAM stability in solution. To the best of the authorsʹ knowledge, this is the first time that the formation of alkanethiols on nanoelectrodes has been reported; with the important distinction that nanografting is a method of backfilling nanoscale pinholes in existing SAMs. It is interesting to find that the rate of film formation is still enhanced on nanoscale electrodes without a template SAM layer that indicates that spatial confinement effects are not the only contributing factors to the increased rate of SAM formation on nanoscale electrodes.

2 | EXPERIMENTAL METHODS

2.1 | Nanoelectrode design and fabrication

The fabrication of Microsquare Nanoband Edge Electrode (MNEE) arrays has been previously reported.[18] In short, an oxidized silicon wafer is coated with nanometer-thick layers of Ti and Pt, 10 nm and 50 nm, respectively, deposited using e-beam and patterned using photolithography. Onto these, a layer of silicon nitride is deposited before a second photolithographic step is used to pattern an array of squares that were etched through to the silicon oxide using a reactive ion etch. This leaves cavities with an electrode band running around the inner walls, see Figure 1. Arrays of 1764 squares 30 μm long and separated by 90 μm (from center to center) were used in this study.

2.2 | Electrode cleaning

Macrodisk Pt electrodes with a diameter of 1.6 mm (geometric area 2.01 mm^2) were obtained from IJ Cambria,

RESEARCH ARTICLE
doi.org/10.1002/elsa.202100077

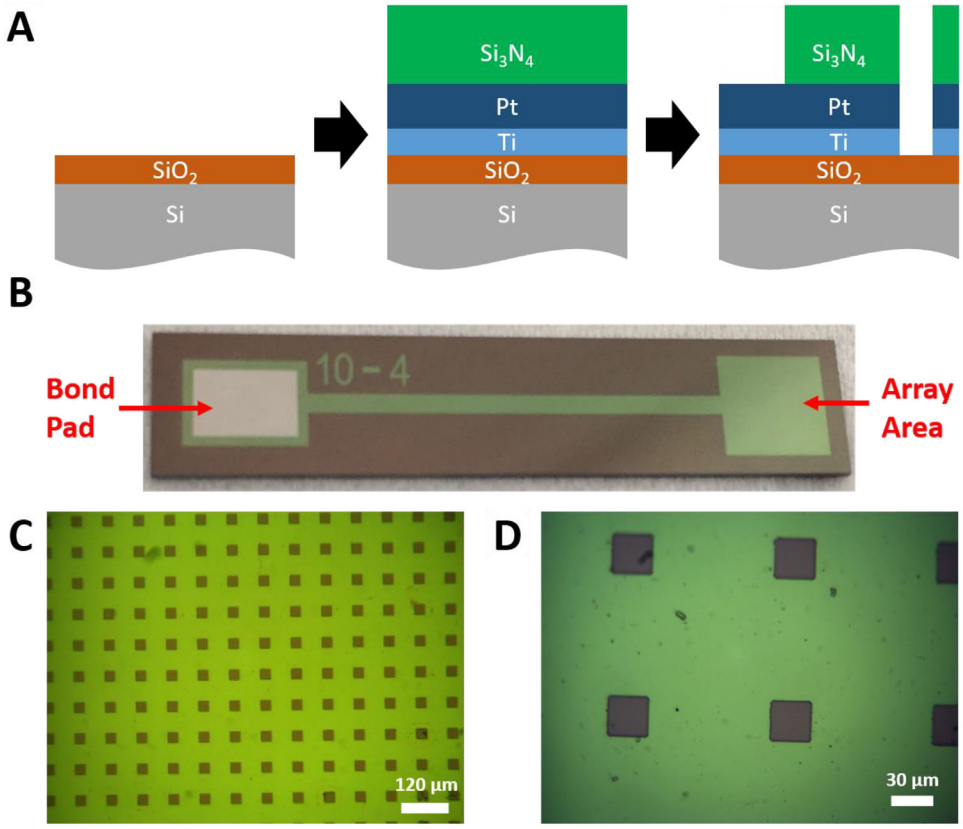

FIGURE 1 (a) Schematic representation, not to scale, showing how the electrodes are fabricated. A silicon wafer with an oxidized surface is coated with nm high layers of Ti (10 nm, as an adhesion layer) and Pt (50 nm) before being coated with a layer of silicon nitride (300 μm thick). The final step is the photolithographic patterning and etching of bond pads and cavities. (b) A labeled photograph of a device, the bond pad. and array area (1 cm^2). (c) Low magnification and (d) high magnification optical image of the nanoelectrode array

Cumbria UK. These were cleaned in piranha solution (WARNING, extremely dangerous, use with extreme caution) made up fresh before each use by mixing concentrated sulfuric acid and hydrogen peroxide (30%) in a 3:1 ratio by volume for 30 s to regenerate the electrode surface. The electrode was then polished in slurries of 1.0 μm, 0.3 μm, and 0.05 μm alumina micro polish (Buehler, IL, USA) consecutively on a polishing micro-cloth (Buehler, IL, USA). Electrochemical cleaning involved cycling between -0.32 V and +1.8 V in 1 M H_2SO_4 (all from Sigma–Aldrich, Cumbria, UK) in ultrapure water (18.2 MΩ/cm, Millipore MilliQ). Cleaning was stopped when the peak currents in a solution of 1 mM potassium ferricyanide and 1 mM potassium ferrocyanide in 10 mM KCl reached the calculated currents for an electrode of this geometry, using the Randles-Sevcik equation and literature diffusion coefficients of 7.26×10^{-6} cm^2/s for ferrocyanide[19] and 6.67×10^{-6} cm^2/s for ferricyanide;[19] the oxidation and reduction peak currents were calculated to be 4.8 μA and 4.5 μA, respectively, at a scan rate of 0.1 V/s, temperature of 25°C (controlled using a water bath built in house). The typical method of calculating the electrode area from the oxide reduction peak area cannot be used here as nanoelectrodes have enhanced diffusion and as such their CVs possess waves and not peaks, see Supporting Information 1B. Cyclic voltammograms of the clean macro and MNEE arrays in 0.1 M H_2SO_4 have been included in Supporting Information 1A and 1B, respectively. It is common practice to integrate the oxygen or hydrogen adsorption/desorption peaks to calculate the electroactive surface area of the clean electrodes. However, this method of analysis is not suitable for the MNEE arrays as the peaks are not easily resolved. This is perhaps best evidenced by the oxygen desorption peak in Supporting Information 1B that merges with the hydrogen adsorption peaks. As a result, the electroactive surface area of the clean electrodes is calculated using other methods. Similar results have been reported on other Pt electrodes by the White group.[20]

2.3 | Electrode functionalization and electrochemical analysis

An SAM formation solution was made consisting of 30 μM 6-mercaptohexan-1-ol (MCH; Sigma–Aldrich,

RESEARCH ARTICLE
doi.org/10.1002/elsa.202100077
Chemistry Europe
European Chemical Societies Publishing

Cumbria, UK), 150 μM tris-(2-carbocyethyl)phosphine (TCEP, Sigma–Aldrich, Cumbria, UK) in a 50:50 mixture of dimethyl sulfoxide (DMSO, Fisher Scientific) and ultrapure water (18.2 MΩ.cm, Millipore MilliQ). For the nanoelectrode array experiments, this solution was diluted by a factor of 1000 to give 30 nM MCH and 150 nM TCEP in 50:50 DMSO:water by volume.

A SAM analysis solution comprising 1 mM potassium ferricyanide and 1 mM potassium ferricyanide with either 10 mM or 100 mM KCl (all from Sigma–Aldrich, Cumbria, UK) was made and degassed for 10 min by sparging with Argon before each experiment was run.

The electrode was dipped in the SAM formation solution for a set time before rinsing with a jet of ultrapure water (18.2 MΩ.cm, Millipore MilliQ) and transferring to the SAM analysis solution. Electrochemical measurements were started as soon as possible after moving to the SAM analysis solution ($t \leq 20$ s). All experiments were run in a three-electrode system using an AUTOLAB PGSTAT 128N (Metrohm, UK) against a saturated calomel reference electrode (SI analytics, Fischer UK) and Pt gauze counter electrode (Sigma–Aldrich, Cumbria, UK). All electrochemical impedance spectroscopy measurements were conducted at the measured open circuit potential with 50 frequencies scanned logarithmically from 100 kHz to 0.1 Hz using a sinusoid with a 10 mV rms peak amplitude. After each measurement the electrode was rinsed with ultrapure water (18.2 MΩ.cm, Millipore MilliQ) and placed back in the SAM formation solution, this process was repeated until the film had reached a steady state. The electrode was left in the SAM formation solution overnight in an evaporation-proof chamber (made in-house) prior to measuring as before in the SAM analysis solution to obtain the saturated film response.

3 | RESULTS AND DISCUSSION

3.1 | Electrochemistry of the clean electrodes

To establish that the electrodes are clean and functional their cyclic voltammograms (CVs) and Nyquist plots (EIS) have been included in Figure 2, alongside the equivalent circuits to which they are fit. The CVs in sulfuric acid (0.1 M) of both the macro- and nanoelectrodes have been included in Supporting Information 1. Due to the enhanced mass transport for nanoelectrodes, their CVs in sulfuric acid display a wave-like response rather than the typical diffusion-limited peak evident in macroscale electrode responses, and as such their CVs cannot be integrated to calculate surface area and determine the cleanliness of the electrodes. Therefore, in order to assess the cleanliness of the electrodes, they were used to determine the diffusion coefficients of potassium ferrocyanide using the Randles-Sevcik equation (Equation 1):

$$i_p = 0.4463nFAc\left(\frac{n\mathrm{F}\upsilon D}{\mathrm{R}T}\right)^{0.5} \quad (1)$$

where i_p is the limiting current (in A), n is the number of electrons being transferred, F is Faraday's constant (in C/mol), A is the area of the electrode (in cm^2), c is the concentration of redox agent in the bulk electrolyte (in mol/cm^3), υ is the scan rate (in V/s), D is the diffusion coefficient (in cm^2/s), R is the universal gas constant (in J K^{-1} mol^{-1}), and T is the temperature (in K), it was possible to calculate the diffusion coefficients for both ferricyanide and ferrocyanide and compare these to literature values.[19] The error was calculated by taking the standard deviation calculated from the diffusion coefficients obtained at each scan rate. It was found using this method that the diffusion coefficient for ferrocyanide was $9.1 \pm 0.3 \times 10^{-6}$ cm^2/s to one standard deviation, this is in good agreement with other literature values.[21] Since Equation 1 is area dependent and the geometric area of the electrode (2.01 mm^2) was used and gave a value of D in good agreement with the literature, it can be concluded that the electrodes are clean. This was done rather than rearranging Equation 1 to determine the area or integrating the sulfuric acid peaks so as to be directly comparable with the nanoelectrode data below.

The limiting current for this array of recessed nanoelectrodes, at fast scan rates where each electrode is acting independently and neighboring diffusion profiles have not begun to overlap (in these arrays >0.05 V/s), has again been established through simulation and experiment and is described by Equation 2:[18a]

$$i_l = 0.956nNFDcL \quad (2)$$

where i_l is the limiting current (in A), n is the number of electrons being transferred, F is Faraday's constant (in C/mol), D is the diffusion coefficient (in cm^2/s), c is the concentration of redox agent in the bulk solution (in mol/cm^3), L is the edge length of one of the squares (in m), and N is the number of squares in the array.

The CVs in Figure 2c were recorded in 10 mM KCl to compare the calculated value of D with the macro electrode data. At the fastest scan rates, the value of D observed on the nanoelectrode array was calculated, using Equation 2, as 7.9×10^{-6} cm^2/s $\pm$ 0.3×10^{-6} cm^2/s; which is similar to the value found for macro electrodes above and consistent with the values reported in the literature.[19] For the nanoelectrode arrays, the EIS data were recorded in 100 mM KCl SAM analysis solution to be able to obtain values of

RESEARCH ARTICLE
doi.org/10.1002/elsa.202100077
Chemistry Europe
European Chemical Societies Publishing

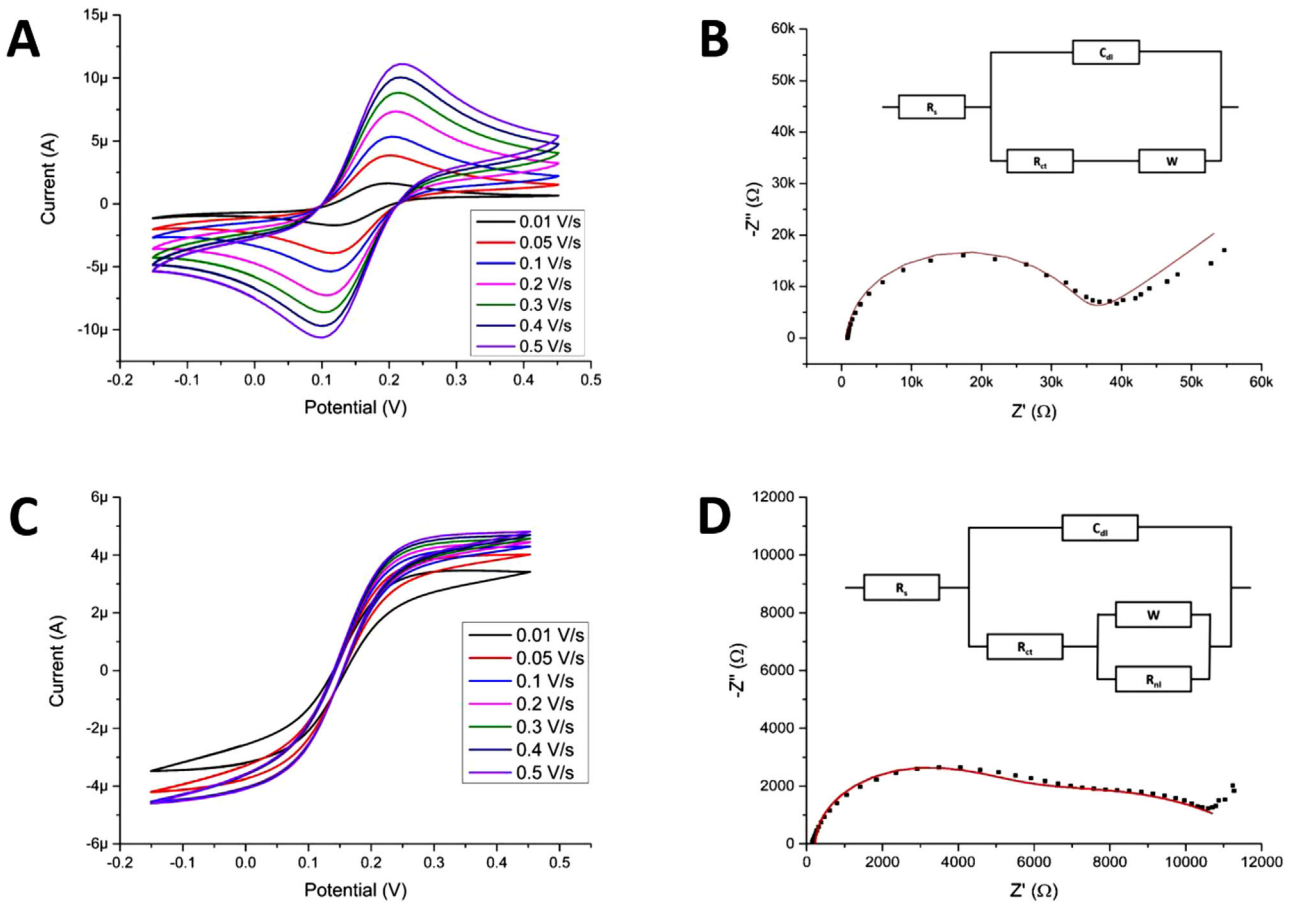

FIGURE 2 Macro electrode cyclic voltammogramms at different scan rates (a) and Nyquist plot (black squares) with the fit (solid red line) to the inset equivalent circuit (b) of clean electrodes. (c) Microsquare nanoband edge electrode (MNEE) array voltammogramms over the same range of scan rates as the macroelectrode and (d) Nyquist plot (black squares) with fit (solid red line) to the inset equivalent circuit. All data were measured in a solution of 10 mM KCl (a, b, and c) or 100 mM KCl (d) with 1 mM potassium ferricyanide, 1 mM potassium ferrocyanide versus a saturated calomel reference electrode and Pt gauze counter electrode. EIS was performed at the open circuit potential (+175 mV). All measurements were performed at 25°C in solutions degassed with argon

R_{ct} and R_{nl} when an SAM was formed, see Figure S3 for the Nyquist plots of the nanoelectrode arrays in 10 mM KCl SAM analysis solution.

Nyquist plots from the EIS measurements of the clean electrodes have been provided in Figure 2b,d; along with their fits to the appropriate equivalent circuits inset in each. In both Nyquist plots, there is a region of poorer fitting at the very lowest frequencies, in Figure 2d, this region corresponds to overlapping diffusion fields in the array over these timescales and this has been excluded from the circuit fitting. In both cases, the longer timescales mean that data in these low-frequency regions are more prone to noise from bulk solution movements and hence do not fit as well. For the macroelectrodes, a good fit to the Randles circuit is observed, fitted parameters can be found in Table S1. For the nanoelectrode arrays, the data fit well to the previously established equivalent circuit,[1e,18a] for fit data see Table S2. A small Warburg-type response caused by linear diffusion to the total array area was excluded from the fitting but can be seen at the lowest frequencies of Figure 2d. In the case of nanoelectrodes, two apparent semi-circles can be resolved, the first is attributed to R_{ct} and the C_{dl}, the second to the formation of a nonlinear (hemispherical) diffusion profile at the nanoelectrode. It was important to establish the cleanliness of the electrodes to show that none of the data trends observed are caused by imperfections or contaminations of the electrode surfaces. By first determining that the macroscale electrodes are clean and then showing that the measurement of physical constants through equations that are related to the area of the electrodes, in this case, the diffusion coefficient of ferricyanide (D) using Equation 2, are identical on both the macro electrodes and the MNEE arrays, we can establish the cleanliness of the electrodes. Establishing what area is available is key to properly understanding the surface coverage and inspiring confidence in the data reported in this work.[9b]

RESEARCH ARTICLE
doi.org/10.1002/elsa.202100077
Chemistry Europe
European Chemical Societies Publishing

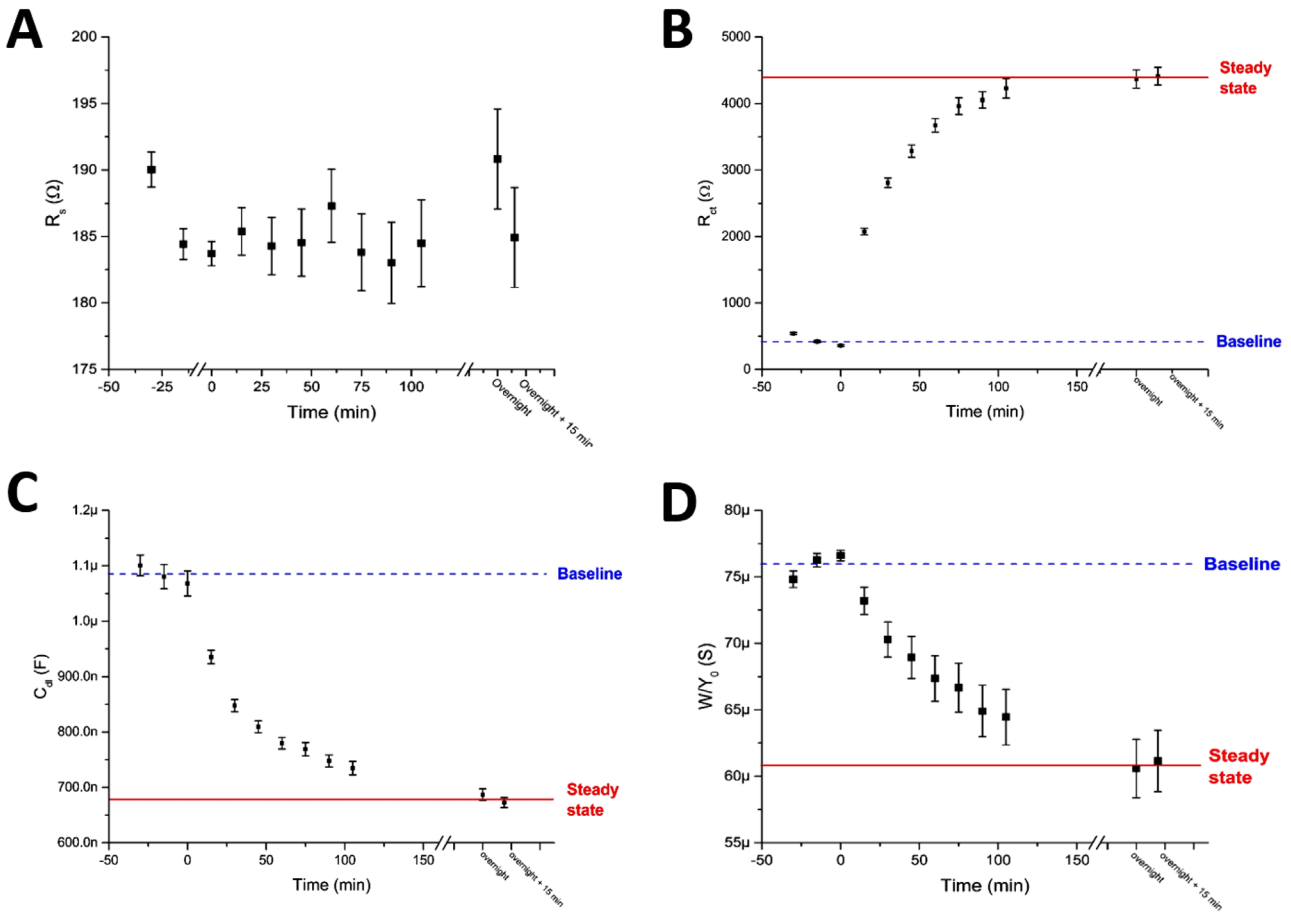

FIGURE 3 Fitted values from Pt macro k_{on} experiments. The film was left to saturate overnight in the SAM formation solution as shown by the red line two measurements were then taken 15 min apart to confirm that the film had reached a steady state. The error bars are from the error in the fit to one standard deviation. All time points below 0s were repeat measurements of a clean electrode in the SAM analysis solution to ascertain the baseline signal

3.2 | Macroelectrode: SAM formation

All macro electrode data were fitted to the Randles' equivalent circuit that allowed us to quantify the: solution resistance (R_s), double layer capacitance (C_{dl}), charge transfer resistance (R_{ct}), and admittance (Y_0, by virtue of modeling as a Warburg element for semi-infinite linear diffusion).[22]

A set of typical results of these experiments are shown in Figure 3a-d, the changes in each of the fitted parameters are discussed in more detail below. A single set of results has been included here for ease of reading, repeat data have been included in the Supporting Information S4. There is some minor variation between electrodes, but the time to saturate and order of magnitude of all fitted values are reassuringly consistent across repeats. It is encouraging from the outset that all the fitted elements, except R_s, are observed to go from a baseline response (obtained from repeat measurements made on clean electrodes and plotted at times below 0 in all figures) to a steady-state SAM response over approximately 2 h, which is in-keeping with other works.[3,5]

It is evident from the data in Figure 3 that the errors increase as the film forms in all fitted parameters except C_{dl}, Figure 3c. Given that this is the only parameter not dependent on the flow of redox agent to the electrode surface, we propose that as the film forms, it impedes the flow of the redox agent to the electrode surface. This could be through either steric hindrance or by changing the solvation and hydrophobicity of the electrode.[23] Despite these increasing errors with increasing SAM coverage, the overall change in the fitted values for all parameters except R_s are significant and will be discussed individually in more detail.

On examining Figure 3a, it can be observed that there is no significant change in R_s caused by MCH binding to the electrode. Since in these experiments the electrode is being taken out of the solution to have thiol successively added, the conductivity of the SAM analysis solution should undergo no significant change. Where $t < 0$ a

RESEARCH ARTICLE
doi.org/10.1002/elsa.202100077
Chemistry Europe
European Chemical Societies Publishing

clean electrode was measured repeatedly in the SAM analysis solution to obtain a baseline signal for the system. The values of R_s remain constant throughout the experiment never deviating significantly from 180 to 195 Ω (3.6-3.9 Ω.cm^2). R_s offers no information as to the SAM film but the consistency across these values evidences the stability of the experimental setup.

Typical fitted values of R_{ct} from these experiments are given in Figure 3b. The formation of the MCH film on the surface causes R_{ct} to increase as the uncoated electrode surface decreases. The fitted values of R_{ct} increase to the steady state after approximately 2 h, during which the values of R_{ct} increased from 500 Ω (10 Ω.cm^2) to 4500 Ω (90 Ω.cm^2) from baseline to equilibrium. This ninefold increase in R_{ct} is the biggest change in any of the fitted circuit elements, making R_{ct} the most sensitive parameter for studying film formation.

Typical fitted values of C_{dl} from these experiments are given in Figure 3c, which shows that the film takes just under 2 h to reach a steady state, with the values dropping by 36% from the baseline, 1.1 μF (0.55 F/m^2) to 0.7 μF (0.35 F/m^2). C_{dl} decreases from the baseline asymptotically approaching the steady state over the 2-h period, the same timescale as was observed for R_{ct} and Y_0. This decrease in C_{dl} can be explained by the decrease in uncoated electrode surface area as a film forms as well as a reduction in the dielectric permittivity at the electrode surface as the water is replaced by MCH.[24]

The fitted value of Y_0 decreases from 76 μS to 61 μS when going from a baseline to a thermodynamic equilibrium, Figure 3d. This equates to a 20% decrease from the baseline to the steady-state value. The admittance follows the same trend as R_{ct} and C_{dl} of asymptotically approaching the steady state over a period of around 2 h. Conceptually, as the electrode coverage by the SAM increases the resistance to charge transfer increases. As the rate of electron transfer decreases a drop in the flux of redox agent to the electrode surface will naturally occur; therefore, a decrease in Y_0 is expected. The authors propose two competing processes that could be decreasing Y_0; either as the film forms the electrode area is decreasing and pinholes in the film still allow diffusion to a smaller active electrode surface area, or the film inhibits the flow of redox agent to the electrode, thereby decreasing the diffusion coefficient and lowering Y_o. It is not known which of these processes is dominating but this warrants further investigation. These trends are all in keeping with the literature both in terms of timescales required and with the accepted theory of SAM formation from solution.[3,16] In all the fitted parameters where a response could be observed, there is a sharp initial increase in signal from that then changes over time to a more resistive conformation as more SAM is added. This fits with the model that an initial physisorption process is followed by a chemisorption process, rearrangement of the SAM to a "standing up" conformation in islands, and a rearrangement of the metal substrate as pits are formed.[4,16] This macroelectrode data can therefore be seen as evidence that this EIS-based approach to analyze film formation provides a wealth of information about the system and is in good agreement with the current state of the art knowledge of metal thiol monolayers.

3.3 | Nanoelectrode array: SAM formation

The equivalent circuit for nanoelectrode arrays, Figure 2d, can be used to quantify the: solution resistance (R_s), capacitance double layer (C_{dl}), charge transfer resistance (R_{ct}), admittance (Y_0, again as a Warburg element), and the resistance to nonlinear diffusion (R_{nl}).[18a] While the initial data for the clean electrodes could be modeled this way, once a film started to form on the electrode, the two distinct hemispheres previously observed could no longer be resolved. This is no doubt due to one of the resistances, either R_{ct} and R_{nl}, increasing much faster than the other. As such the data were fit as a single apparent semi-circle. This gives values of R_s that is the same as before, R_x that is the sum of R_{ct} and R_{nl}, and Y_0 from a constant phase element. The constant phase element was required as the imaginary components of the impedance data were a combination of the capacitance from the high-frequency hemisphere (C_{dl}) and the admittance (Y_0/W) from the low-frequency hemisphere. This means that it is not possible to directly compare the values of the macro- and nanoelectrode data for the different circuit elements; however, the profiles of the responses over time are of interest.

Rs stays relatively constant over the course of the experiment, as would be expected. The value of R_x was seen to increase linearly with time reaching a steady state in under 100 s, Figure 4b. The linear rate of change indicates a zero-order rate dependency, the rate of formation is independent of the amount of film formed, and there is effectively no k_{off}. It is of interest that the linear fit does not pass through the origin, this would suggest that there is a separate initial process that is followed by this linear increase in resistance over time. The authors interpret this as evidence of a model of instantaneous stochastic film formation, followed by a period of film re-arrangement to a thermodynamic steady state. On the macroelectrode, this rearrangement was observed to take place over 2 h; whereas on the nanoelectrodes, this process is much faster, reaching completion in under 2 min.

If the SAM formation was measured in the same solution in which the SAM was being formed, the SAM formation process might be limited by the flux of MCH to the elec-

RESEARCH ARTICLE
doi.org/10.1002/elsa.202100077
Chemistry Europe
European Chemical Societies Publishing

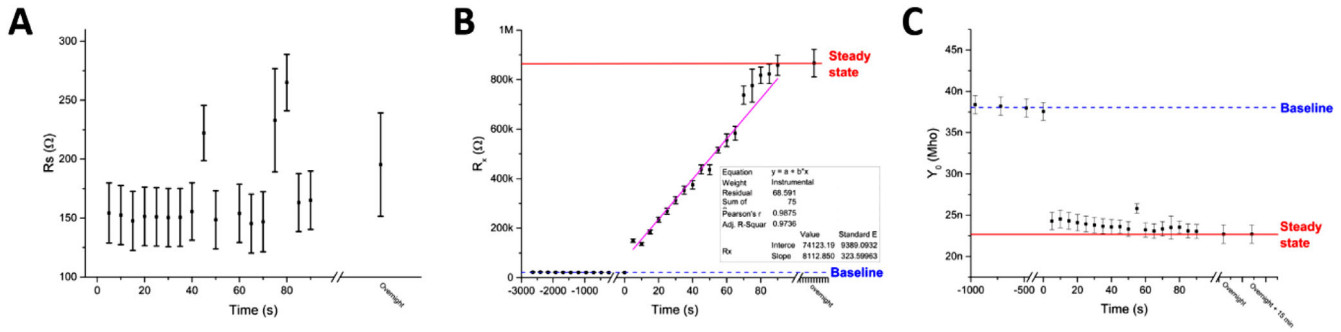

FIGURE 4 Plots of (a) R_s versus time, (b) R_x versus time, and (C) Y_0 versus time; including a baseline obtained by taking repeat measurements of a 30 μm 3D MNEE array in 10 mM SAM analysis solution as shown in all the time points below 0s. The kinetic experiments were performed as described in the experimental section until a steady state was reached as indicated by the red line. All errors given are the errors in the fits given to one standard deviation. The magenta line is a linear fit through all the non-zero time-points measured, excluding the overnight steady-state R_x value

trode surface. By placing in the SAM formation solution for a short a period of time then taking a measurement in an MCH-free solution, there will always be a ready supply of MCH at the electrode surface and the rate of film formation will be entirely dependent on the SAM structure at the interface. To establish that the MNEE SAM formation is not limited by the mass transport of MCH to the electrode surface, we can calculate the mass transport controlled flux (j) of MCH to the MNEE arrays. This has previously been expressed through Equation 3:[18a]

$$j = \frac{\mathrm{BNDc}L}{4\mathrm{N}t\mathrm{L}} \tag{3}$$

where B = 0.956, N is the number of micro-square cavities in the array (1764 in this instance), D is the diffusion coefficient of mercaptohexanol ($4.8 \times 10^{-6}\ cm^2 s^{-1}$)[25], c is the concentration of MCH, L is the edge length of one of the cavities (30 μm), and t is the thickness of the Pt band (50 nm). In Equation 3, 4NtL is the geometric electrode array area. Given that in this instance the SAM was formed in 30 nM MCH, this would give a flux of 7.5×10^{-12} mol cm^2 s^{-1}. Since a well packed MCH SAM has a density on the order of 10^{-9} mol/cm^2,[26] we would anticipate that the MNEE array would take hundreds to thousands of seconds if the mass transport of MCH was limiting the formation process. The macroelectrode formation process takes so long that it is not reasonable to assume the process is limited by the flux of MCH to its surface.

The concentration of MCH in the SAM formation solution was 30 μM for the macroelectrodes but 30 nM for the nanoelectrodes. This 1000-fold dilution was done in order to keep the flux of MCH roughly constant over the two electrode sizes. On the nanoelectrodes, the depletion zone over 5 s will have progressed over a length, $\mathrm{L} = (2Dt)^{\frac{1}{2}} = 7 \times 10^{-3}$cm, which equates to a volume of approximately 7×10^{-7} cm^3 (assuming that the depletion zone is a hemisphere with radius L whose volume is defined as $\mathrm{V} = (2/3)\pi\mathrm{L}^3$). A solution of this volume containing 30 nM MCH will contain 2×10^{-22} moles of MCH, given that the active electrode surface area of each cavity is 6×10^{-6} cm^2; if all the MCH in the depletion zone were to bind to the electrode there would be a surface coverage of roughly 4×10^{-10} cm^2.

In the case of the macroelectrodes, the depletion layer will have progressed 7×10^{-3}cm; however, there will not be hemispherical but linear diffusion in this instance. The number of moles within this distance of the macro electrode surface will be $(3 \times 10^{-8}\mathrm{mol/cm}^3) \times (7 \times 10^{-3}\mathrm{cm}) = 2 \times 10^{-10}$moles/cm^2. The flux was kept constant over the different sizes of electrodes to ensure that the only differences between them are due to the rearrangement of the SAM on the respective electrode surfaces.

While there is an explanation in the literature as to why there is enhanced SAM formation rates on nano-pores due to spatial-confinement effects,[16] that explanation only holds for films that are already in a steady state conformation that have thiols removed and then backfilling is seen to occur at an enhanced rate. Here, the electrodes start off as clean and so there is no template for the thiols to bind into.

We therefore propose another possible explanation based on comparing the bulk to edge ratios of the macro- and nanoelectrodes. At the edge of the electrodes, the SAM is in what Poirier et al[4] termed the "ε-phase" where it is bound through its thiol group to the electrode surface; but the alkane chain and the head group can move between a "standing-up" or "lying-down" position. These thiols overhang the edge of the electrode and experience van der

RESEARCH ARTICLE
doi.org/10.1002/elsa.202100077
Chemistry Europe
European Chemical Societies Publishing

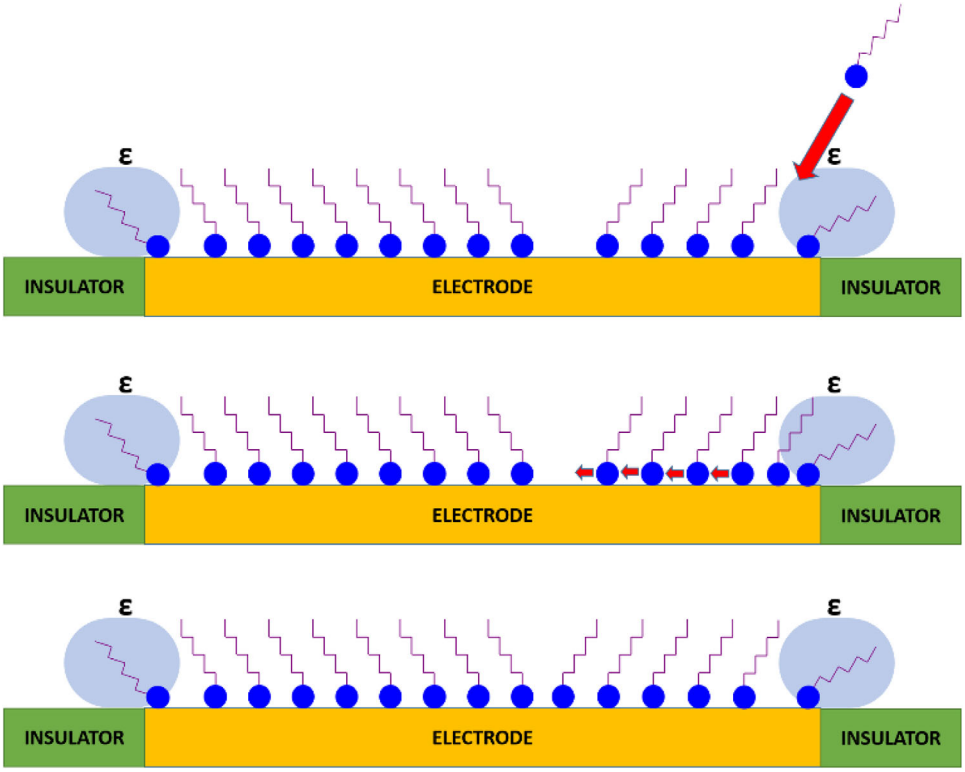

FIGURE 5 Schematic representation (not to scale) of the proposed mechanism of film densification where an incoming MCH molecule can bind at the ε-phase SAM on the edge of the electrode causing the electrode bound thiols to translocate and fill pinholes in the bulk of the film

Waals interactions with the silicon nitride or titanium in the electrode structure or the neighboring thiols in the SAM, see Figure 5.

For nanoscale electrodes, there is a larger proportion of the SAM in this phase as proportionally more of the electrode is edge than in the macroelectrodes. This difference in steady-state SAM structure may allow the film to reach said steady state faster. The rate of desorption of SAMs from a metal surface is relatively slow given the strength of the Pt-S bond. It may be that in the case of the macro electrodes the film rearrangement is influenced by the desorption of MCH during the re-arrangement process, whereas there is no observable k_{off} on the nanoscale electrodes because they are measured over such small time scales.

The fitted values of Y_0, given in Figure 2b show that there is an instantaneous decrease from the baseline to the steady state. This is in agreement with the model of rapid stochastic film formation that re-arranges to a more resistive conformation. The presence of all phases over the entire electrode will still change the dielectric permittivity (ε_r), subsequent re-arrangement must have a minimal effect on the magnitude of ε_r.

As the different phases re-arrange to the most thermodynamically stable φ-phase, the sulfur head groups migrate closer to each other[8b]; in the φ-phase, the sulfur head groups are more closely packed than any of the preceding phases. This densification of the film causes the impedance to increase. In order for more thiol to bind to the surface, it must approach pinholes in the monolayer or alkanethiols in the ε-phase where binding sites are available. The increased ratio of ε-phase MCH on the nanoelectrodes because of the increased edge to bulk ratio, means that theoretically this densification process would be faster for the nanoelectrode array devices. An incoming thiol could bind at the edge of the electrode and the bulk bound molecules can reconfigure to a more stable conformation by translocating on the electrode surface. On a macroelectrode, this reconfiguration process will take longer as a greater proportion of the electrode is bulk rather than the edge. A cartoon depicting this process is given in Figure 5. The MCH would theoretically bind preferentially to the ε-phase because it provides less steric hindrance to an incoming molecule. Pinholes are perhaps better described as unoccupied binding sites as they can encompass those sites blocked by "lying-down" alkanethiols. This is in keeping with STM studies reported by Zhang et al[7a] where the SAM molecules on the edge of an Au(111) terrace were observed to have lower binding energy than those in the bulk of the terrace.

RESEARCH ARTICLE
doi.org/10.1002/elsa.202100077
Chemistry Europe
European Chemical Societies Publishing

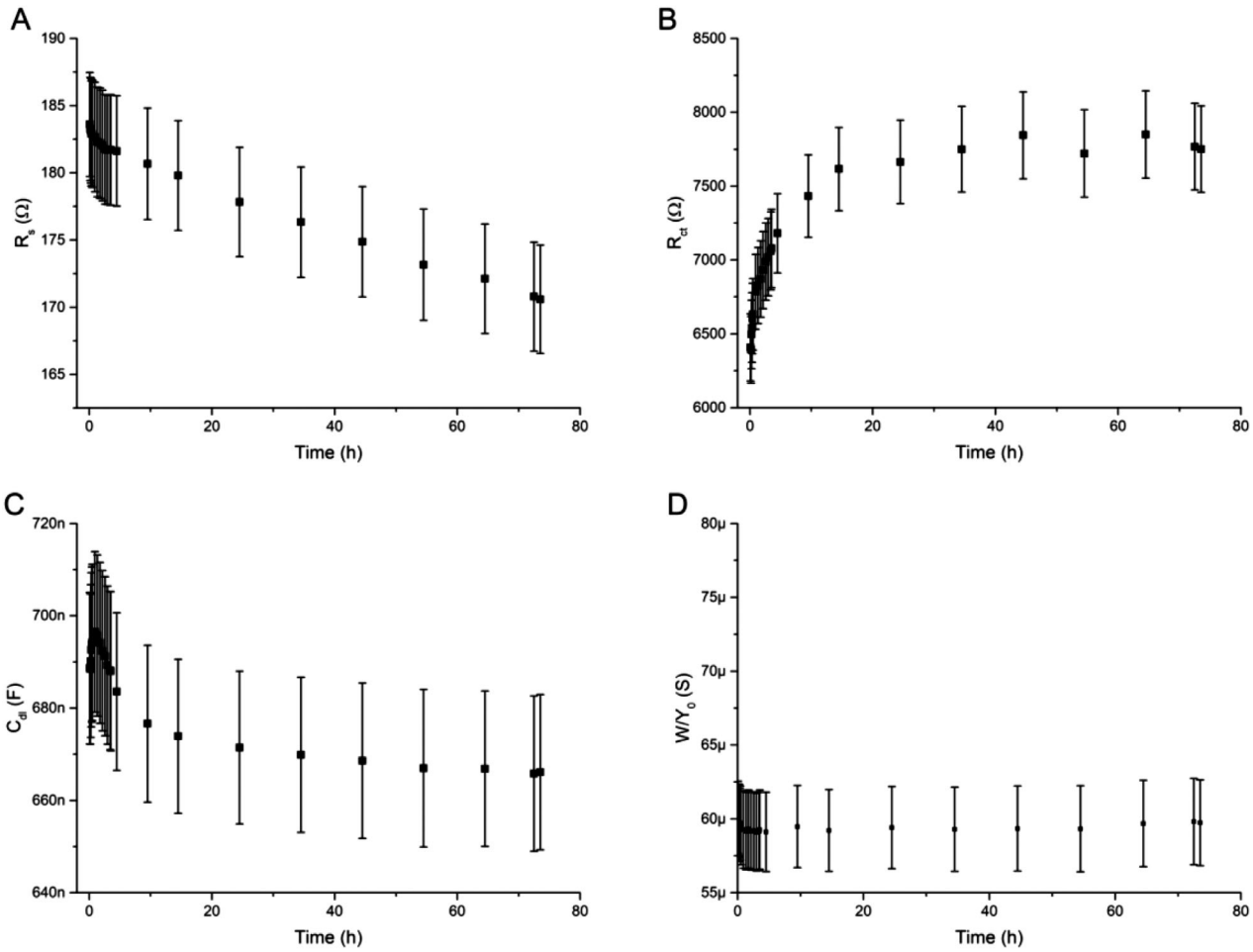

FIGURE 6 Fitted parameters of a macroelectrode (a) Rs, (b) Rct, (c) Cdl, and (d) Y_0; after SAM formation measured over 72 h at a stable temperature of 298 Kelvin in a degassed solution that was kept oxygen-free during the course of the experiments by sparging

3.4 | Subsequent SAM stability in solution

On both macro- and nanoelectrodes, the stability of the resultant SAMs was similar so are reported and discussed together. Figure 6 shows the fitted values for the SAM on a macroelectrode for 72 h and Figure 7 shows the corresponding data for a nanoelectrode for the same period of time. These data were collected by leaving the electrode with a formed SAM layer in SAM analysis solution and taking repeated EIS measurements, the system was held at a stable temperature (25°C) in an oxygen-free environment.

There is a small decrease in Rs over time, which can be attributed to minor changes in the solution over long periods of time, such as evaporation increasing the effective concentration of redox agent and supporting electrolyte. As stated earlier, R_s offers no information on the film and has only been included for completeness and to inspire confidence in the experimental setup.

The resistance of the system is seen to vary greatly over the 72 h measurement but always undergoes a significant increase in Rct or Rx, (Figures 6c and 7b, respectively). It is interesting to note that the values of R_{ct} never drop below the value of the steady-state response measured during the SAM formation. Thus, the SAM does not appear to be desorbed from the electrode surface. This is further supported by the observation that there is no change in the C_{dl} or Y_0 during these measurements, Figure 6c,d, respectively.

This slow change in R_{ct} could be driven by switching from the SAM formation solution to being left in the SAM analysis solution.[10a,23b] To test this, experiments were run using the MNEE array in SAM measurement buffers with different KCl concentrations, see Figure 7a-c. A change in electrolyte concentration could theoretically lead to a difference in solvation of the SAM that might cause a rearrangement; however, no change in the temporal stability could be observed in these experiments.

Given the timescale of these experiments, there will naturally be some evaporation of the measurement solution that might increase the salt concentration to the point where it might "crash out" on and block the electrode. Theoretically, this would happen faster in the 100 mM KCl

RESEARCH ARTICLE
doi.org/10.1002/elsa.202100077
Chemistry Europe
European Chemical Societies Publishing

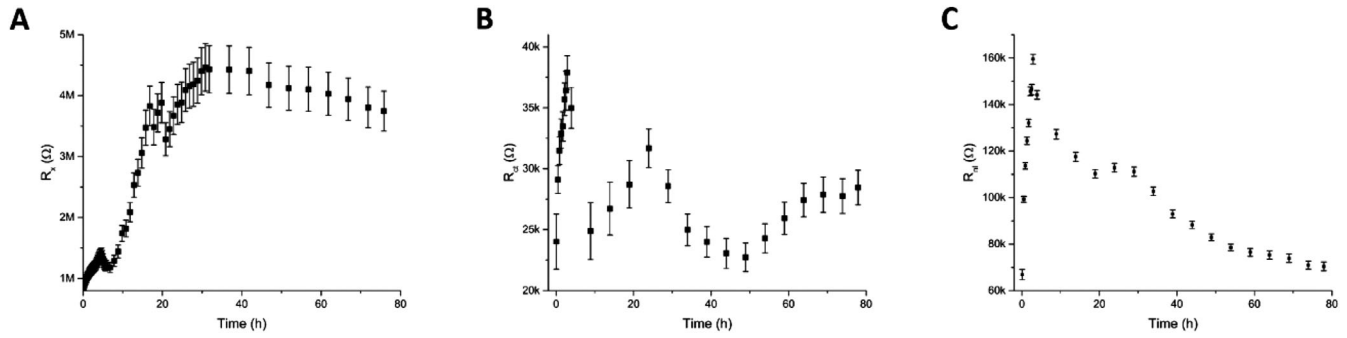

FIGURE 7 Fitted parameters of a microsquare nanoband edge electrode arrays values of (a) Rx, (b) Rct, and (c) Rnl; after SAM formation measured over 72 h at a stable temperature of 298 Kelvin in a degassed solution that was kept oxygen-free during the course of the experiments by sparging. Panel (a) was recorded in a SAM analysis solution containing 10 mM KCl, whereas Panels (b) and (c) were recorded in an SAM analysis solution containing 100 mM KCl.

measurement solutions, Figure 7b,c, since this was not observed and the K_{sp} of KCl is 3.5 M, the salting out of KCl on the electrodes can be ruled out as a possible explanation of the observed trends in Figures 6 and 7.

The true nature of what is occurring over the hours and days following SAM formation is not explained here but warrants further investigation. The practical relevance of these findings is large, this densification of the SAM could easily be misinterpreted as a probe-target binding event in a sensor surface made with a thiolated SAM. These data demonstrate the absolute necessity of assay development in the field to be published with adequate control data to interrogate the stability of the SAM layer and make sure that the attribution of signal changes to probe-target binding (e.g., DNA-DNA hybridization or antibody-antigen recognition) are in fact correct. The authors would like to indicate that reporting the temporal instability of SAMs is not novel,[2a,10a,12] but the fact that the same instability is seen on nanoelectrodes is novel and interesting. These findings mean that whatever is the cause of this instability, the different SAM structure on nanoelectrodes does not influence or reduce it. Any postulated theories as to the source of this instability should take this into consideration. Since this final finding has been reported for the Pt-S system, there may be some doubt cast on its relevance to Au-S systems, which are more commonly used for biosensing systems. However, the long-term instability of the Au-S interface has also previously been reported on macroscopic electrodes.[7c,10b,12]

4 | CONCLUSIONS

For the first time, the differences in SAM formation and stability on macro- and nanoelectrodes have been studied electrochemically. It was found that MCH SAMs formed on nanoelectrodes reach a thermodynamic equilibrium in a matter of seconds to minutes using 1000 times more dilute MCH than the macroelectrode. This is a clear advantage for the use of nanoelectrode sensors as the probe molecules put down in a SAM layer can be prohibitively expensive. EIS has been used to investigate the mechanism of film formation and suggests that the enhanced rate of film formation on the nanoelectrode array may be down to the ability of the film to respond to increases in stress. This is the ability of the film to cope with a proposed densification process as a result of the increased edge-to-bulk ratio of nanoelectrodes compared to macroelectrodes.

Analysis of the stability of an MCH monolayer once it has been moved to an aqueous SAM analysis solution showed that there is a period over which the film becomes more resistive. This process occurs on a timescale of hours and is not sensitive to changes in the ionic strength of the SAM analysis solution. These random changes were observed on both macro- and nanoelectrodes so are not dependent on the electrode geometry or dimensions.

The change in the electrochemistry of the film should be of particular note to researchers in the field who develop assays on metal thiolate films, which can often take several hours to run, as any changes in electrochemistry they observe may in fact be these random changes in the SAM films reported here rather than specific changes due to probe-target hybridization. As such adequate controls and repetitions of experiments should be routinely included in any such experiments.

CONFLICT OF INTEREST

The authors declare no conflict of interest.

ACKNOWLEDGMENTS

A.P. would like to acknowledge the University of Edinburgh Schools of Chemistry and Engineering for funding this work.

REFERENCES

1. a) N. Wisniewski, F. Moussy, W. M. Reichert, *Fresenius J. Anal. Chem.* **2000**, *366*, 611-621; b) G. Plicchi, E. Marcelli, L. Cercenelli, *Journal of Mechanics in Medicine and Biology* **2006**, *6*, 81-89; c) C. S. Smith, C. M. Bowie, K. D. Song, H. Yoon, V. K. Varadan, W. K. Kim, in *Nanosensors, Biosensors, and Info-Tech Sensors and Systems 2011*, *Vol. 7980* (Ed.: V. K. Varadan), **2011**; d) A. G. Zestos, *International Journal of Electrochemistry* **2018**; e) A. Piper, B. Alston, D. Adams, A. R. Mount, *Faraday Discuss.* **2018**.
2. a) T. Wink, S. J. van Zuilen, A. Bult, W. P. van Bennekom, *Analyst* **1997**, *122*, R43-R50; b) J. L. Hammond, N. Formisano, P. Estrela, S. Carrara, J. Tkac, *Essays Biochem* **2016**, *60*, 69-80; c) P. Quan Li, A. Piper, I. Schmueser, A. R. Mount, D. K. Corrigan, *Analyst* **2017**, *142*, 1946-1952.
3. C. M. A. Brett, S. Kresak, T. Hianik, A. M. O. Brett, *Electroanalysis* **2003**, *15*, 557-565.
4. G. E. Poirier, *Langmuir* **1999**, *15*, 1167-1175.
5. H. Hakkinen, *Nat. Chem.* **2012**, *4*, 443-455.
6. C. E. D. Chidsey, G. Y. Liu, P. Rowntree, G. Scoles, *J. Chem. Phys.* **1989**, *91*, 4421-4423.
7. a) J. Zhang, C. J. Ulstrup, *Langmuir* **2006**, *22*, 6203-6213; b) F. P. Zamborini, R. M. Crooks, *Langmuir* **1997**, *13*, 122-126; c) D. Grumelli, F. L. Maza, K. Kern, R. C. Salvarezza, P. Carro, *J. Phys. Chem. C* **2016**, *120*, 291-296.
8. a) E. E. Bedford, S. Boujday, V. Humblot, F. X. Gu, C. M. Pradier, *Colloids and Surfaces B-Biointerfaces* **2014**, *116*, 489-496; b) S. Xu, S. J. N. Cruchon-Dupeyrat, J. C. Garno, G. Y. Liu, G. K. Jennings, T. H. Yong, P. E. Laibinis, *J. Chem. Phys.* **1998**, *108*, 5002-5012; c) S. Xu, G.-Y. Liu, *Langmuir* **1997**, *13*, 127-129.
9. a) A. W. H. Lee, D. Kim, B. D. Gates, *Appl. Surf. Sci.* **2018**, *436*, 907-911; b) A. Makaraviciute, X. X. Xu, L. Nyholm, Z. Zhang, *ACS Appl. Mater. Interfaces* **2017**, *9*, 26610-26621.
10. a) L. Srisombat, A. C. Jamison, T. R. Lee, *Colloids and Surfaces a-Physicochemical and Engineering Aspects* **2011**, *390*, 1-19; b) L. J. Cristina, G. Ruano, R. Salvarezza, J. Ferrón, *J. Phys. Chem. C* **2017**, *121*, 27894-27904.
11. N. Camillone, C. E. D. Chidsey, G. Liu, G. Scoles, *J. Chem. Phys.* **1993**, *98*, 4234-4245.
12. G. Mani, D. M. Johnson, D. Marton, V. L. Dougherty, M. D. Feldman, D. Patel, A. A. Ayon, C. M. Agrawal, *Langmuir* **2008**, *24*, 6774-6784.
13. a) E. Y. Katz, *J. Electroanal. Chem. Interfacial Electrochem.* **1990**, *291*, 257-260; b) E. Y. Katz, A. A. Solov'ev, *Anal. Chim. Acta* **1992**, *266*, 97-106; c) A. A. Solov'ev, E. Y. Katz, V. A. Shuvalov, Y. E. Erokhin, *Bioelectrochem. Bioenerg.* **1991**, *26*, 29-41.
14. G. M. Whitesides, J. K. Kriebel, J. C. Love, *Sci. Prog.* **2005**, *88*, 17-48.
15. a) D. L. Bu, S. Riechers, J. Liang, G. Y. Liu, *Nano Res.* **2015**, *8*, 2102-2114; b) E. A. Josephs, J. R. Shao, T. Ye, *Nanoscale* **2013**, *5*, 4139-4143; c) D. L. Bu, T. J. Mullen, G. Y. Liu, *Acs Nano* **2010**, *4*, 6863-6873.
16. S. Xu, P. E. Laibinis, G.-Y. Liu, *J. Am. Chem. Soc.* **1998**, *120*, 9356-9361.
17. a) H. Häkkinen, *Nat. Chem.* **2012**, *4*, 443; b) H. Guesmi, N. B. Luque, E. Santos, F. Tielens, *Chemistry-a European Journal* **2017**, *23*, 1402-1408; c) E. Bedford, V. Humblot, C. Methivier, C. M. Pradier, F. Gu, F. Tielens, S. Boujday, *Chemistry-a European Journal* **2015**, *21*, 14555-14561; d) X. Torrelles, E. Pensa, E. Cortes, R. Salvarezza, P. Carro, C. H. Guerrero, C. Ocal, E. Barrena, S. Ferrer, *J. Phys. Chem. C* **2018**, *122*, 3893-3902.
18. a) I. Schmueser, A. J. Walton, J. G. Terry, H. L. Woodvine, N. J. Freeman, A. R. Mount, *Faraday Discuss.* **2013**, *164*, 295-314; b) J. G. Terry, I. Schmueser, I. Underwood, D. K. Corrigan, N. J. Freeman, A. S. Bunting, A. R. Mount, A. J. Walton, *IET Nanobiotechnol.* **2013**, *7*, 125-134.
19. S. J. Konopka, B. McDuffie, *Anal. Chem.* **2002**, *42*, 1741-1746.
20. a) H. Ren, S. R. German, M. A. Edwards, Q. Chen, H. S. White, *J. Phys. Chem. Lett.* **2017**, *8*, 2450-2454; b) B. Zhang, Y. Zhang, H. S. White, *Anal. Chem.* **2004**, *76*, 6229-6238.
21. a) K. Ngamchuea, S. Eloul, K. Tschulik, R. G. Compton, *J. Solid State Electrochem.* **2014**, *18*, 3251-3257; b) H. S. Harned, R. M. Hudson, *J. Am. Chem. Soc.* **1951**, *73*, 5083-5084.
22. a) A. J. Bard, L. R. Faulkner, *Electrochemical methods : fundamentals and applications*, Wiley, New York; Chichester, **1980**; b) E. Gileadi, *Physical Electrochemistry-Fundamentals, Techniques and Applications*, WILEY-VCH Verlag GmbH & Co. KGaA, Weinheim, Federal Republic of Germany, **2015**; c) D. K. Corrigan, H. Schulze, G. Henihan, A. Hardie, I. Ciani, G. Giraud, J. G. Terry, A. J. Walton, R. Pethig, P. Ghazal, J. Crain, C. J. Campbell, K. E. Templeton, A. R. Mount, T. T. Bachmann, *Analyst* **2013**, *138*, 6997-7005.
23. a) M. Zolk, F. Eisert, J. Pipper, S. Herrwerth, W. Eck, M. Buck, M. Grunze, *Langmuir* **2000**, *16*, 5849-5852; b) J. J. Calvente, R. Andreu, *PCCP* **2010**, *12*, 13519-13521; c) R. L. C. Wang, H. J. Kreuzer, M. Grunze, *J. Phys. Chem. B* **1997**, *101*, 9767-9773.
24. a) N. Tercero, K. Wang, R. Levicky, *Langmuir* **2010**, *26*, 14351-14358; b) C. Berggren, P. Stalhandske, J. Brundell, G. Johansson, *Electroanalysis* **1999**, *11*, 156-160; c) E. Barsoukov, J. R. Macdonald, Second edition /ed., Wiley-Interscience, Hoboken, N.J., **2005**, pp. 1 online resource (xvii, 595 pages). d) F. C. Bedatty Fernandes, M. S. Goes, J. J. Davis, P. R. Bueno, *Biosens. Bioelectron.* **2013**, *50*, 437-440.
25. J. J. Calvente, R. Andreu, L. González, M.-L. A. Gil, J. D. Mozo, E. Roldán, *J. Phys. Chem. B* **2001**, *105*, 5477-5488.
26. A. Makaraviciute, X. Xu, L. Nyholm, Z. Zhang, *ACS Appl. Mater. Interfaces* **2017**, *9*, 26610-26621.

SUPPORTING INFORMATION

Additional supporting information may be found in the online version of the article at the publisher's website.

How to cite this article: Andrew Piper, Damion K. Corrigan, Andrew R. Mount. *Electrochem Sci Adv*. **2021**, e2100077. https://doi.org/10.1002/elsa.202100077